XL CILAMCE
IBERO-LATIN AMERICAN CONGRESS ON COMPUTATIONAL METHODS IN ENGINEERING
NOVEMBER 11-14, 2019
Praiamar Natal Hotel & Convention
Natal, RN-BRAZIL

MODELING AND SIMULATION OF THE CONCENTRATION OF SPECIES FOR A DIRECT ETHANOL FUEL CELL

Marcelo M. De Souza
marcelo.maraschin@ifsc.edu.br
Instituto Federal de Santa Catarina
Rua Heitor Villa Lobos, 222, Lages, 88506-400, Santa Catarina, Brasil
Ranon S. Gomes
ranon@unifap.br
Universidade Federal do Amapá
Rod. Juscelino Kubitschek, km 2 - Jardim Marco Zero, Macapá, 68903-419, Amapá, Brasil
Álvaro L. De Bortoli
dbortoli@mat.ufrgs.br
Universidade Federal do Rio Grande do Sul
Avenida Bento Gonçalves, 9500, Porto Alegre, 91509-900, Rio Grande do Sul, Brasil

Abstract. The generation of energy is a subject in constant debate, either for its efficiency and renewability or for the emission of pollutants. In addition, energy consumption has grown over the years, and fossil fuels, which account for around 80% of the world's energy generation, run the risk of becoming scarce. A technology with renewable features that has proven to be promising and more efficient than traditional power generators is the fuel cell, making the process clean and efficient. The fuel cell is an electrochemical device that directly converts chemical energy into electricity. In this work, a numerical model is developed for fuel cells with proton exchange membrane and fed by ethanol. The model takes into account the flow, the variation of the concentration of chemical species, the rate of passage of ethanol through the membrane and the overpotential losses in the anode and the cathode. In addition, the concentration of each species is modeled according to the current density of the fuel cell. The finite element method is used to calculate the flow and concentration of the species in different layers of the cell (inlet and outlet channels, diffusion layer and catalyst layer). The Crank-Nicolson method is used for time discretization. Overpotential losses are calculated using parameters obtained with the numerical model. These losses can be estimated by calculating the activation, the ohmic polarization and the concentration overpotentials. The flow results, the variation of the species concentration, passage of the ethanol through the membrane and the limiting current density are shown. Results of cell voltage are compared for different catalysts and temperatures with experimental data found in the literature.

Keywords: Direct Ethanol Fuel Cell, Mathematical modeling, Overpotential losses.

1 Introduction

Energy sources are classified as renewable and non-renewable. Non-renewables are represented by fossil fuels such as oil, natural gas and coal. These are the most used fuels in the world, accounting for about 80% of the used energy. The burning of these fuels contributes directly to greenhouse gases, global warming and acid rain. In addition, non-renewable energy sources are at risk of scarcity, as energy consumption has increased over time. According to the International Energy Agency, if the average consumption in recent decades is not reduced, world reserves of oil and natural gas may be exhausted. In order to reverse this situation, studies have focused on clean and renewable energy sources. Among the main sources there is hydroelectric, wind, solar and biomass.

Besides this discussion about the use of renewable energy or not, another point is extremely important: the efficiency in the transformation of energy. Currently, internal combustion engines are primarily responsible for the transformation of energy [1]. In some traditional electric power generation systems, the fuel is initially burned to produce heat; then this heat is converted into mechanical energy and finally into electricity. One device that more efficiently uses the available energy sources is the fuel cell [2]. A fuel cell is an electrochemical device that converts the chemical energy present in fuels directly into electrical energy. It provides clean energy and high efficiency in a wide variety of applications [3].

Fuel cells have attracted the interest of researchers and industries in recent years, as they stand out for their high reliability, low noise emission, higher efficiency compared to internal combustion engines, flexibility in size or shape, low emission of pollutants to the atmosphere, among others [4]. Fuel cells are promising devices for use in a variety of applications, such as automobiles, electronic devices, space missions, stationary power generation, drones, and small boats. Due to the great interest in these applications, investment in fuel cell research has increased considerably over the past few years.

Much of the work developed for fuel cells has focused on hydrogen-powered cells. Methanol has also gained interest in recent decades as an alternative fuel to hydrogen. However, hydrogen still requires efficient technologies for its storage and distribution, and methanol is toxic to humans [5]. A promising fuel that has gained considerable interest in recent years is ethanol, which is a renewable fuel that can be produced from biomass.

Many articles have been published proposing the use of ethanol in fuel cells discussing many aspects regarding the materials that should be used to obtain the best performance of the cell [6–9]. However, the papers do not discuss mathematical models for the flow and concentration of chemical species. That is, parameters such as velocity and concentration are used as constants in the calculations of overpotential losses.

Abdullah et al. (2014) reviewed the modeling and simulation of direct ethanol fuel cells (DEFCs) and reported that there are few papers discussing two-dimensional models for them. Therefore, among the main advances in the development and improvement of DEFCs cited by Abdullah et al. (2014), is the development of multiphase and multidimensional mathematical models that can capture the complex physico-chemical behavior of real DEFCs [11].

2 Direct Ethanol Fuel Cell

Proton exchange membrane fuel cells (PEMFCs) have attracted great interest, especially in the automotive industry. They are considered the most promising and are in the highest development stage; it is believed to be the first type of cell to be produced on large scale. PEM fuel cells are attractive because they operate at low temperatures (up to 373 K) [12].

The efficiency of the PEMFC system is generally greater than 50%, i.e. higher compared to internal combustion engines, which have about 30% efficiency with gasoline and 50% with diesel. In addition, fuel cells provide low noise and low vibration.

The PEMFCs bring expectations of not only delivering high energy density and extended run time compared to what the batteries already provide, but also offer the convenience of instant recharge. It is more practical to increase the energy density of a PEMFC without the need to stacking many heavy

batteries in a massive and complex energy system.

PEMFCs can also be classified according to the fuel used (hydrogen, methanol or ethanol). Hydrogen cells are the most used in applications. Afterwards, fuel cells with direct methanol were the main development targets, but due to the toxicity of this fuel, their use on a large scale can cause serious problems [13, 14]. Thus, the interest in direct ethanol fuel cells (DEFC) has grown considerably due to the higher energy density of ethanol, it is less toxic than methanol, it is produced from renewable sources, has less rate of fuel passage through the membrane and affects cathode performance less than methanol [15, 16]. DEFC is considered a promising source of energy [14].

A DEFC is formed by an anode, a cathode and a polymeric membrane. The anode and the cathode are formed by collector plates, the diffusion layer and the catalyst layer. The MEA (Membrane Electrode Assembly) is formed by the diffusion layer, catalyst and membrane: the set consists of the electrodes (anode and cathode). The electrodes consist of layers deposited on a substrate, covered by a catalytic layer.

DEFC functionality follows that of PEMFC, i.e., a fuel is oxidized electrochemically at the anode, generating protons and electrons, while oxygen is reduced at the cathode [2]. The ethanol/water mixture is inserted into the anode side, which reacts to form carbon dioxide, protons and electrons. The protons pass to the cathode through the membrane and the electrons through an external circuit, providing some potential difference. On the cathode side, air/oxygen reacts with the protons and electrons provided by anode to produce water vapor [17].

The electrochemical reactions that occur inside the cell are given by [16]:

$$\mathrm{C_2H_5OH} + 3\mathrm{H_2O}_l \rightarrow 2\mathrm{CO_2} + 12\mathrm{H}^+ + 12e^- \quad \text{at the anode,} \tag{1}$$

$$3\mathrm{O_2} + 12\mathrm{H}^+ + 12e^- \rightarrow 6\mathrm{H_2O}_g \quad \text{at the cathode,} \tag{2}$$

corresponding to the following global reaction,

$$\mathrm{C_2H_5OH} + 3\mathrm{O_2} \rightarrow 2\mathrm{CO_2} + 3\mathrm{H_2O}_g. \tag{3}$$

Complete oxidation of ethanol is complicated by the difficulty in breaking the C-C bonds to form intermediates which are adsorbed on the surface of the catalyst. Generally, the electro-oxidation of ethanol into fuel cells is done using bi-metallic or tri-metallic catalysts with platinum. Goel and Basu 2015 proposed a three-step mechanism for the electrooxidation of ethanol using the PtRu/C catalyst:

$$\mathrm{C_2H_5OH} + \mathrm{Pt} \rightarrow (\mathrm{C_2H_5OH})_{ad,\mathrm{Pt}} \rightarrow (\mathrm{CH_3CHO})_{ad,\mathrm{Pt}} + 2\mathrm{H}^+ + 2e^- \tag{4}$$

$$3\mathrm{H_2O} + 3\mathrm{Ru} \leftrightarrow 3(\mathrm{OH})_{ad,\mathrm{Ru}} + 3\mathrm{H}^+ + 3e^- \tag{5}$$

$$(\mathrm{CH_3CHO})_{ad,\mathrm{Pt}} + 3(\mathrm{OH})_{ad,\mathrm{Ru}} \rightarrow 2\mathrm{CO_2} + 7\mathrm{H}^+ + 7e^- + \mathrm{Pt} + 3\mathrm{Ru}. \tag{6}$$

In the first step, ethanol is adsorbed on the surface of the cell catalyst, releasing electrons and protons. In step two, the dissociation of water occurs in the ruthenium catalyst. In step three, the interaction between the two adsorbed species forms carbon dioxide.

3 Mathematical Model

The model used in this work considers the following hypotheses:

- Two-dimensional flow;
- Incompressible fluid;
- Well hydrated membrane;
- Catalyst poisoning is neglected;
- Acetaldehyde and carbon dioxide are the main products of the electrochemical reactions at the anode;
- Use of atmospheric air at the cathode;
- Single-phase flow at anode and cathode;

- CO_2 is totally dissolved in the liquid.

On the sides of the anode and cathode, the equations have the same shape, and are given by the continuity, amount of movement and conservation of species.

On both sides (anode and cathode), the fuel cell is divided into three parts: input/output channels (Ω_1 and Ω_6), diffusion layer (Ω_2 and Ω_5) and catalyst layer (Ω_3 and Ω_4), where $\Omega = \Omega_1 \cup \Omega_2 \cup \Omega_3 \cup \Omega_4 \cup \Omega_5 \cup \Omega_6$ is the cell domain. Figure 1 shows the parts of the domain.

Figure 1. DEFC domain

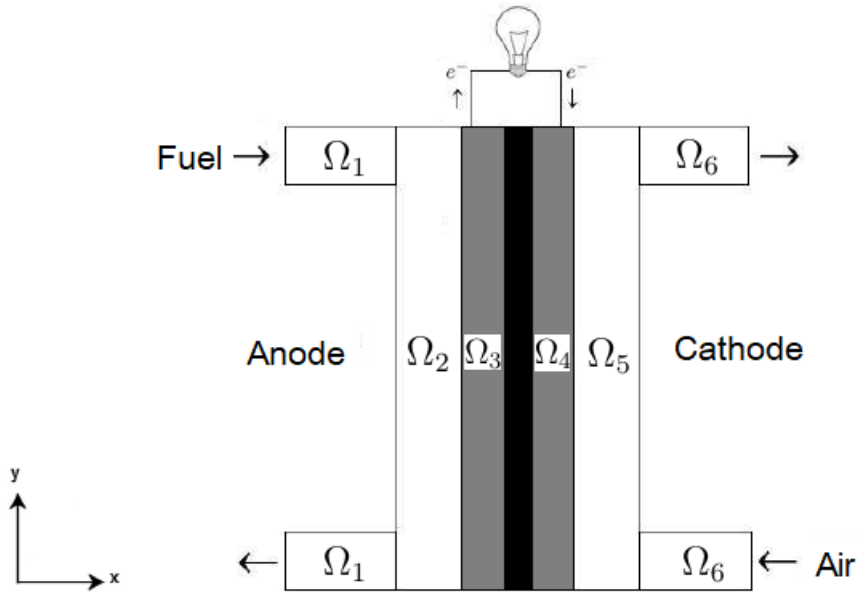

The momentum equation is composed of transient, convective, diffusive, pressure gradient and a source term, as follows

$$\rho\frac{\partial \mathbf{u}}{\partial t} - \mu D_\varepsilon \nabla^2 \mathbf{u} + \rho \mathbf{u}\cdot\nabla\mathbf{u} + \nabla p = \rho S_u \quad \text{in } (0,\tau]\times\Omega, \tag{7}$$

$$\mathbf{u}(0;x,y) = \mathbf{u}_0 \text{ in } \Omega, \tag{8}$$

where $\mathbf{u} = (u_1, u_2)$ is the velocity, μ the viscosity, p the pressure and τ the final time of operation. The specific mass ρ is constant at the anode ρ_a and at the cathode ρ_c, the dynamic viscosity is given by μ_a at the anode and μ_c at the cathode. The specific mass and the dynamic viscosity of the ethanol/water mixture in the anode are chosen according to the temperature (Table 1), in the same way for atmospheric air at the cathode (Table 2).

Table 1. Specific mass (ρ) and viscosity (μ) at the anode for ethanol concentration of 1 M and given initial operating temperature [18].

Temperature (K)	ρ_a (g cm^{-3})	μ_a (g cm^{-1}s^{-1})
333	0.8591	0.005064
348	0.8454	0.004057
373	0.8224	0.002721

Table 3 shows the porosity correction factor D_ε and the source term S_u, where ε_{dl} and ε_{cl} are the porosities of the diffusion and catalyst layers, respectively, and κ is the permeability. The source term S_u

Table 2. Specific mass (ρ) and viscosity (μ) at the cathode for given initial temperature [18].

Temperature (K)	ρ_c (g cm^{-3})	μ_c (g cm^{-1}s^{-1})
333	0.001156	0.0002252
348	0.001107	0.0002330
373	0.001042	0.0002438

is added in the different layers of the porous medium to describe the flow of the fluid through a porous medium [19].

Table 3. Source term S_u and porosity correction factor D_ε.

	Input/output channel	Diffusion layer	Catalyst layer
D_ε	1	$2,25\left(\frac{1}{\varepsilon_{dl}}-1\right)^2$	$2,25\left(\frac{1}{\varepsilon_{cl}}-1\right)^2$
S_u	0	$-\varepsilon_{dl}\frac{\mu}{\kappa}\mathbf{u}$	$-\varepsilon_{cl}\frac{\mu}{\kappa}\mathbf{u}$

The mass conservation equation can be expressed by [20]

$$\rho\nabla\cdot\mathbf{u}=\dot{m}\quad \text{in } (0,\tau]\times\Omega, \tag{9}$$

where $\dot{m}$ is the source term, that in the anodic catalyst is due to the consumption of ethanol and water, the passage of ethanol through the membrane and the generation of carbon dioxide, and in the cathodic catalyst is due to the generation of water, the consumption of oxygen and the generation of carbon dioxide due to the oxidation reaction of the ethanol [21]. In the other layers of the cell, $\dot{m}$ is zero, that is, incompressibility is assumed in every fuel cell, except for the catalysts. The values of $\dot{m}$ in the catalysts are given in Table 4.

Table 4. Source term $\dot{m}$.

	Catalyst layer at the anode	Catalyst layer at the cathode
$\dot{m}$	$S_{\text{EtOH}}+S_{\text{H}_2\text{O}}+S_{\text{CO}_2}$	$S_{\text{H}_2\text{O}}+S_{\text{O}_2}+\frac{2M_{\text{CO}_2}}{7F}j^p_{\text{xover}}$

The equation of the species can be written as [22]

$$\rho\frac{\partial X_k}{\partial t}+\rho\mathbf{u}\cdot\nabla X_k-\rho D_k^{\text{eff}}\nabla^2 X_k=S_k,\qquad \text{with}\quad \sum_k X_k=1. \tag{10}$$

where X_k is the molar fraction of the species $k=\{\text{EtOH},\text{H}_2\text{O},\text{O}_2,\text{CO}_2\}$, D_k^{eff} is the effetive difusivity coefficient and S_k is the source term. S_k is zero in the input and output channels, and in the diffusion layer; in the catalyst layer is given by Tables 5 and 6, where j^p_{xover} is the pseudo current density due to the passage of ethanol through the membrane [19, 23]. M_{EtOH}, M_{H_2O}, M_{O_2} and M_{CO_2} are the molecular weights of ethanol, water, oxygen and carbon dioxide, respectively.

Table 5. Source term S_k in the anode catalyst layer.

	Ethanol	Water	Carbon dioxide
S_k	$-\frac{M_{\text{EtOH}}}{2F}(j+j^p_{\text{xover}})$	$-\frac{M_{\text{H}_2\text{O}}}{F}j$	$\frac{2M_{\text{CO}_2}}{7F}j$

Table 6. Source term S_k in the cathode catalyst layer.

	Oxygen	Water
S_k	$-\frac{M_{O_2}}{4F}(j + j^p_{\text{xover}})$	$\frac{M_{H_2O}}{2F}(j + j^p_{\text{xover}})$

The molar fractions of the acetaldehyde at the anode and the nitrogen at the cathode are given, respectively, by [24]:

$$X_{CH_3CHO} = 1 - X_{EtOH} - X_{H_2O} - X_{CO_2}, \tag{11}$$

$$X_{N_2} = 1 - X_{O_2} - X_{H_2O}. \tag{12}$$

The current density of the cell, J, is defined as follows:

$$J = \int_0^{\delta_{cl}} j dx, \tag{13}$$

where δ_{cl} is the thickness of the catalyst layer. Similarly is made for J_c, J_{xover}, J_0.

The effective diffusivity is given by [21]

$$D_k^{\text{eff}} = D_k \varepsilon^{3/2}, \tag{14}$$

where ε is the porosity and D_k is the diffusion coefficient of the kth component.

The molar concentrations of the species k can be obtained by the molar fraction as follows [25]:

$$C_k = \frac{\rho X_k}{M}, \tag{15}$$

where ρ is the specific mass of solution and M is the mean molar mass of the solution.

3.1 Ethanol Crossover

The passage of ethanol through the membrane is caused by diffusion and electro-osmotic drag, and is calculated as follows [6, 11]:

$$J_{\text{xover}} = \frac{C_{EtOH} e^{\frac{v_m}{k_m}}}{e^{\frac{v_m}{k_m}} - 1} v_m \tag{16}$$

where $v_m = M P_{EtOH}/\rho_a$ is the surface velocity of the ethanol in the membrane, with the coefficient of transport of ethanol through the membrane described by [21]

$$P_{EtOH} = P_{H_2O} \frac{C_{EtOH}}{C_{H_2O}} \tag{17}$$

where C_{EtOH} and C_{H_2O} are the concentrations of ethanol and water at the interface between the anode catalyst and the membrane, and $P_{H_2O} = \sigma J/F$ is the transport of water through the membrane, with σ the coefficient of electro-osmotic drag of water on the membrane and $k_m = D_{EtOH,m}/\delta_m$ the coefficient of mass transfer of ethanol into the membrane. The pseudo current density, due to the passage of ethanol through the membrane is given by

$$J^p_{\text{xover}} = J_{\text{xover}} nF, \tag{18}$$

where n is the number of electrons transferred in electro-oxidation.

4 Overpotential losses

The total cell voltage can be obtained using the following expression:

$$V_{cell} = E^0_{cell} - (\eta_{act} + \eta_{ohm} + \eta_{con}), \tag{19}$$

where η_{act} are the losses due to the activation, which is the sum of the losses in the anode and the cathode, that is, $\eta_{act} = \eta_{act,a} + \eta_{act,c}$; η_{ohm} are the losses due to ohmic resistance and η_{con} are the losses due to the concentration, which is also the sum of the losses in the anode and the cathode, $\eta_{con} = \eta_{con,a} + \eta_{con,c}$. E^0_{cell} is the theoretical potential of DEFC, which is approximately 1.14 V.

The model equation for the overpotential concentration at the anode is given by [7]:

$$\eta_{con,a} = \left(\frac{RT}{\alpha_a nF}\right) \ln\left(\frac{J}{J_0\left(e^{\frac{|\mathbf{u}|}{k_d}} + B\right)}\right), \tag{20}$$

where B is a constant,

$$B = \frac{J}{nF|\mathbf{u}|C_{\text{EtOH}}\left(e^{|\mathbf{u}|/k_d}((u/k_f)+1)\right) - 1}, \tag{21}$$

with C_{EtOH} the concentration of ethanol in the catalyst layer, $\mathbf{u}$ the average velocity in the anode catalyst calculated by Eq. (7) and the mass transfer coefficient of ethanol is given by

$$k_d = \frac{D^{\text{eff}}_{\text{EtOH}}}{\delta_{dl,a}}, \tag{22}$$

where $\delta_{dl,a}$ is the thickness of the anode diffusion layer and k_f [26] is given by:

$$k_f = 1,87 \times 10^{-4}\left(\frac{J}{0,003}\right)^{0,32}. \tag{23}$$

The expression for the overpotential of concentration at the cathode is given by [7, 11]:

$$\eta_{con,c} = \left(\frac{RT}{\alpha_c nF}\right) \ln\left(\frac{J_c}{J_0(1 - J_c N)}\right), \tag{24}$$

where $J_c = J + J_{\text{xover}}$, α_c is the charge transfer coefficient at the cathode and N is a constant defined by

$$N = \frac{\delta_{dl,c} C_{\text{O}_2}}{nF D^{\text{eff}}_{\text{O}_2}}, \tag{25}$$

with C_{O_2} the oxygen concentration and $D^{\text{eff}}_{\text{O}_2}$ the effective diffusivity of oxygen in the porous medium.

A relation between the overpotential of activation and the current density at the anode was reported in the work of Pramanik and Basu (2010). This relation is derived from the rates of the electrochemical reactions and the expression for the constant rate of reactions given by Bard and Faulkner (2001), thus the overpotential of activation at the anode is given by:

$$\eta_{act,a} = \frac{RT}{\alpha_a nF} \ln\left[\frac{J(C_{\text{EtOH}} C_{\text{H}_2\text{O}})^{-0.25}}{K_{\text{EtOH}}}\right], \tag{26}$$

where C_{H_2O} and C_{EtOH} are the concentration of water and ethanol in the catalyst layer, respectively, and K_{EtOH} is a global parameter for the oxidation of ethanol.

Losses by activation at the cathode can be obtained from the Tafel equation [16, 28, 29], resulting in:

$$\eta_{act,c} = \frac{RT}{\alpha_c nF} \ln\left(\frac{J_c}{J_0}\right). \tag{27}$$

The ohmic losses are expressed according to Ohm's law and can be described as [7]

$$\eta_{ohm} = J\left(\frac{\delta_m}{\sigma_m} + R_b\right), \tag{28}$$

where $R_b = 0,006\ \Omega\ \text{cm}^2$ is the specific area of resistance of the electrodes, δ_m is the thickness of the membrane and σ_m is the ionic conductivity that is given by [7]

$$\sigma_m = (0,005139\theta - 0,00326)\exp\left[1268\left(\frac{1}{303} - \frac{1}{T}\right)\right], \tag{29}$$

where θ is the hydration of the Nafion membrane.

The parameters used to solve the equations of the model for the DEFC are listed in Table 7 and Table 8.

Table 7. Parameters used in the model for a DEFC.

Parameter	Unit	Value	Reference
κ_a	cm^2	1.76×10^{-7}	[30]
κ_c	cm^2	1.0×10^{-7}	[30]
δ_m (Nafion 117)	cm	0.01778	[31]
δ_m (Nafion 115)	cm	0.001145	[7]
$\delta_{cl,a}$	cm	0.001	[9]
$\delta_{cl,c}$	cm	0.001	[9]
$\delta_{dl,a}$	cm	1	[11]
$\delta_{dl,c}$	cm	1	[11]
ε_{cl}	dimensionless	0.4	[31]
α_c	dimensionless	1	[8]
σ	dimensionless	3.16	[7]
n	dimensionless	12	Eq. (1)
D_{CO_2}	$\text{cm}^2\ \text{s}^{-1}$	1.92×10^{-5}	[32]
K_{EtOH}	Coulomb $(\text{mol cm})^{-0.5}\ \text{s}^{-1}$	1	[33]

Table 8. Temperature dependent parameters for the catalysts of a DEFC.

Temperature (K)	Catalyst	α_a	J_0 (mA cm^{-2})	Reference
373	Pt/C	0.0369	0.48	[34]
333	PtRu/C	0.036	0.39917	[35]
348	PtRu/C	0.04	0.683	[35]
373	PtSn/C	0.0505	5.7	[34]

5 Numerical Results

In this work, the finite element method was used for the discretization of the equations in space, using triangles and the Crank-Nicolson method for time discretization [36].

A 10 cm high fuel cell, approximately 4 cm long, with diameter of the 1 cm inlet/outlet channels and the catalyst area of 50 cm^2 was considered. The thickness of the diffusion layers, catalysts and the membrane are given in Table 7.

Figure 2 shows the mesh used to simulate the fuel cell. The mesh was chosen for solution variation of less than 5%.

Figure 2. Mesh for fuel cell.

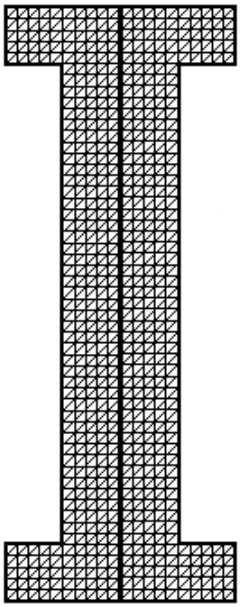

A regular increment was used with $h = 0.2$ cm, that is, 2358 degrees of freedom for each velocity component, each chemical species and temperature, and 488 degrees of freedom for pressure. The velocity and chemical species approximations are quadratic, and the approximation for pressure is linear. The final simulation time is $T = 30$ min and the time step is $\Delta t = 0.1$ s.

The mathematical model for fuel cells requires initial and boundary conditions. The conditions are defined for a fuel cell according with the domain given by Fig. 1. The initial conditions ($t = 0$ s) on the anode side are presented in Table 9 for ethanol concentration of 1 M and flow rate of 1 ml min^{-1}, and for the cathode in Table 10 considering the flow rate of 120 ml min^{-1}.

Table 9. Initial conditions on the anode side.

Parameter	Value
Velocity (u_1)	0.02 cm s^{-1}
Pressure (p)	1 bar
Mole fraction of ethanol (X_{EtOH})	0.25
Mole fraction of water ($X_{\mathrm{H_2O}}$)	0.75
Mole fraction of carbon dioxide ($X_{\mathrm{CO_2}}$)	0

Table 10. Initial conditions on the cathode side.

Parameter	Value
Velocity (u_1)	2.55 cm s^{-1}
Pressure (p)	1 bar
Mole fraction of oxygen (X_{O_2})	0.21
Mole fraction of water (X_{H_2O})	0

The boundary conditions on the input channel of the fuel cell, on the anode side, are

$$u_1 = 0.02 \text{ cm s}^{-1}; u_2 = 0; \frac{\partial p}{\partial x} = 0; X_{EtOH} = 0.25; X_{H_2O} = 0.75; X_{CO_2} = 0, \tag{30}$$

and on the outlet channel they are

$$\frac{\partial u_1}{\partial x} = 0; \frac{\partial u_2}{\partial x} = 0; p = 1 \text{ bar}; \frac{\partial X_{EtOH}}{\partial x} = 0; \frac{\partial X_{H_2O}}{\partial x} = 0; \frac{\partial X_{CO_2}}{\partial x} = 0. \tag{31}$$

The boundary conditions on the input channel on the cathode side are

$$u_1 = 2.55 \text{ cm s}^{-1}; u_2 = 0; \frac{\partial p}{\partial x} = 0; X_{O_2} = 0.21, X_{H_2O} = 0, \tag{32}$$

and on the output channel they are

$$\frac{\partial u_1}{\partial x} = 0; \frac{\partial u_2}{\partial x} = 0; p = 1 \text{ bar}; \frac{\partial X_{O_2}}{\partial x} = 0; \frac{\partial X_{H_2O}}{\partial x} = 0. \tag{33}$$

and for all other boundaries of the fuel cell the velocity is zero. The pressure and the species have the Neumann condition equal zero.

5.1 Mole fraction of species

The hypotheses used in the simulations of this section were:

- Catalyst of PtRu/C at the anode and Pt/C at the cathode [7];
- Flow rate of 1 ml min^{-1} at the anode [6];
- Flow rate of 120 ml min^{-1} at the cathode [6];
- Initial pressure of 1 bar [8];
- Temperature of 348 K;
- Initial concentration of ethanol of 1 M;
- Current density of 90 mA cm^{-2};
- Final time of $\tau = 30$ min [37];
- Membrane Nafion 117 [31];
- Diffusion layer porosity of $\varepsilon_d = 0.65$ [9].

Figure 3 and Fig. 4 show the molar fraction of the species at the anode (ethanol, water and carbon dioxide) and at the cathode (oxygen and water vapor), respectively, operating at current density equal to 90 mA cm^{-2}. The molar fractions are presented throughout the fuel cell domain. The molar fractions of ethanol (Fig. 4(a)) and water (Fig. 4(b)) decrease close to the catalyst wall due to electro-oxidation reactions, exactly where there is formation of by-products such as carbon dioxide (Fig. 4(c)), for example. The mole fraction of oxygen (Fig. 5(a)) decreases and there is water vapor formation (Fig. 5(b)) on the cathode side. There are differences in the anode and cathode isolines. This is due to the physical state of the fluid (liquid at the anode and gaseous at the cathode).

Figure 3. Molar fractions of ethanol, water and carbon dioxide on the anode side of the DEFC for current density of 90 mA cm^{-2} and ethanol concentration of 1 M.

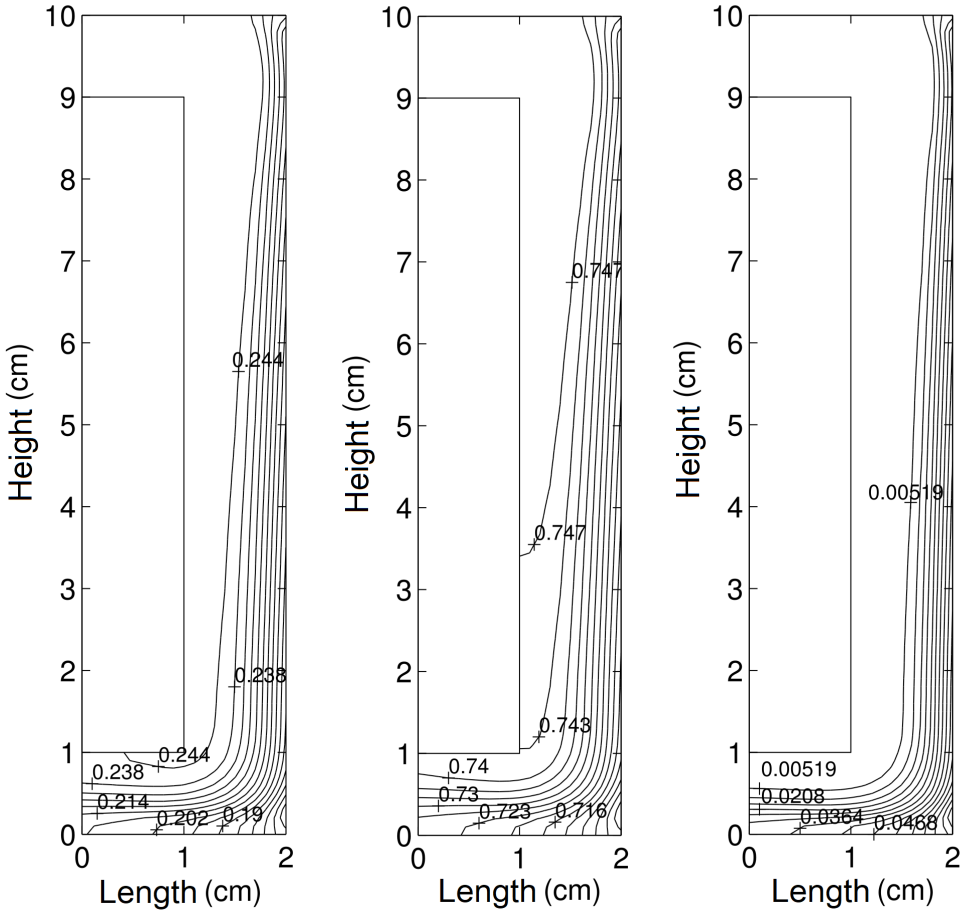

(a) Molar fraction of ethanol (b) Molar fraction of water (c) Molar fractions of carbon dioxide

5.2 Limiting Current Density

The limiting current density is the current density value when the ethanol concentration in the anodic catalyst layer goes to zero [9], that is, when there is no more fuel in the anode catalyst in order to carry out the reactions of electro-oxidation. Limiting current density will always occur, but are observed more easily when small concentrations of ethanol (less than 1 M) are inserted, since the limiting current density will also be low. In this section, a result using ethanol concentration of 0.25 M is presented.

The hypotheses used in the simulations of this section were:

- Catalyst of PtSn/C at the anode and Pt/C at the cathode [9];
- Flow rate of 1.36 ml min^{-1} at the anode [9];
- Flow rate of 120 ml min^{-1} at the cathode [6];
- Initial pressure of 1 bar [8];
- Temperature of 363 K;
- Initial concentration of ethanol of 0.25 M;
- Final time of $\tau = 30$ min [37];
- Membrane Nafion 115 [7];
- Diffusion layer porosity of $\varepsilon_d = 0.65$ [9].

Figure 4. Molar fractions of oxygen and water vapor on the cathode side for current density of 90 mA cm^{-2}.

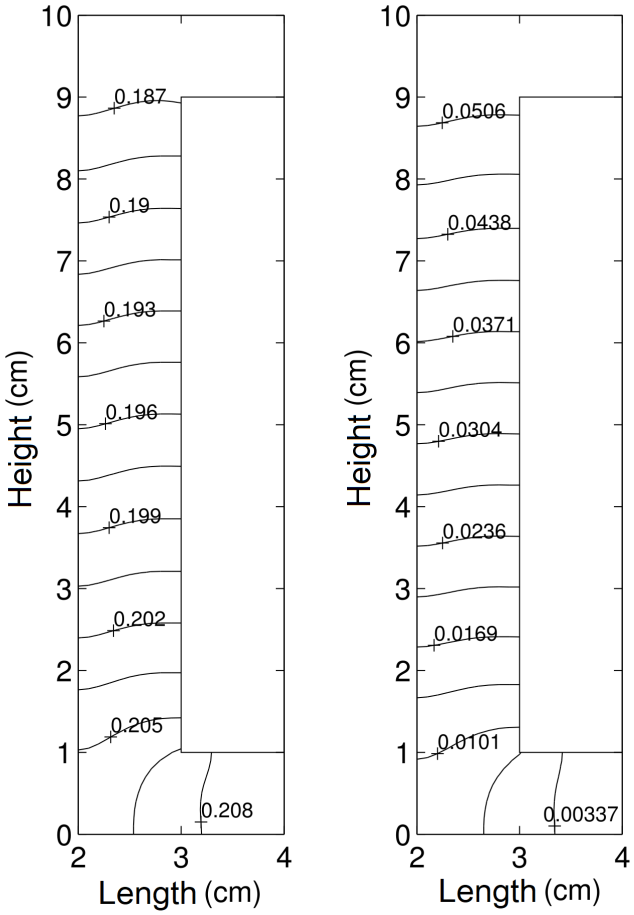

(a) Molar fractions of oxygen (b) Molar fractions of water vapor

In Fig. 5 are presented three results of molar fraction of ethanol for three current densities: 100 mA cm^{-2}, 150 mA cm^{-2} and 174 mA cm^{-2}. The cell was fed with 0.25 M ethanol. It is observed that with the current densities of 100 mA cm^{-2} (Figure 6(a)) and 150 mA cm^{-2} (Figure 6(b)), despite the low molar fraction of ethanol, fuel is still present near the cell catalyst. However, with the current density of 174 mA cm^{-2} the values closely approximate zero (0.0032) at the bottom of the catalyst, characterizing the limiting current density of 174 mA cm^{-2}, as presented by Suresh and Jayanti [9] in their article.

5.3 Catalyst influence

The anode catalyst may be the most important element in the study of direct ethanol fuel cells, as it directly affects the efficiency of the device. In addition, the catalyst is responsible for much of the cost of this device, since the main and most efficient catalysts utilize platinum in its composition. In the numerical model, the catalysts strongly affect the results, since they modify the transfer coefficients at the anode (α_a) and at the cathode (α_c) and also the reference current density (j_0).

The hypotheses used in the simulations of this section were:

- Catalyst of Pt/C at the cathode [7];
- Catalysts at the anode: PtSn/C [34] and Pt/C [34];
- Flow rate of 1 ml min^{-1} at the anode [6];

Figure 5. Molar fraction for ethanol concentration of 0.25 M, temperature of 363 K and flow in the anode of 1.36 ml min^{-1}

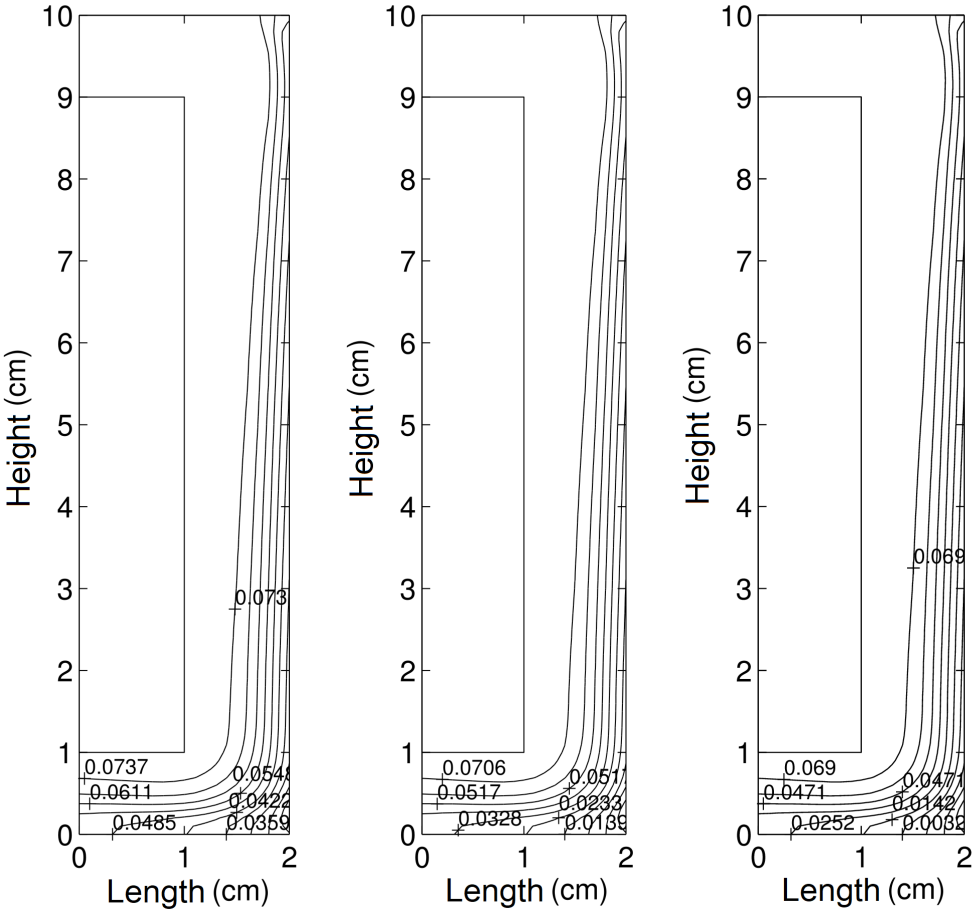

(a) Current density of 100 mA cm^{-2}. (b) Current density of 150 mA cm^{-2}. (c) Current density of 174 mA cm^{-2}.

- Flow rate of 120 ml min^{-1} at the cathode [6];
- Initial pressure of 1 bar [8];
- Temperature of 373 K [34];
- Initial concentration of ethanol of 2 M;
- Final time of $\tau = 30$ min [37];
- Membrane Nafion 117 [31];
- Diffusion layer porosity of $\varepsilon_d = 0.65$ [9].

In Fig. 6 the model is used to compare two types of catalysts for the anode, which used experimental data for comparison [34, 38]. In both cases, we observed similarity of the experimental data with the values of the numerical simulation. The relative error with the PtSn/C catalyst is 7.78% and with the Pt/C catalyst is 8.96%. For each catalyst, the performance of the fuel cell can be attributed to the kinetics of the reactions of the electrodes, both by oxidation of ethanol at the anode and by reduction of oxygen at the cathode. A better yield is observed with the PtSn/C catalyst, since the tin prevents membrane poisoning by intermediate species and improves the catalytic activity of platinum [39]. As expected, catalysts of the Pt/C type do not perform well in DEFCs, due to the difficulty of breaking the C-C bonds.

Figure 6. Comparison of the cell voltage for two types of catalysts using a temperature of 373 K. The experimental data of the catalysts of PtSn/C and Pt/C are from Tayal et al. (2012).

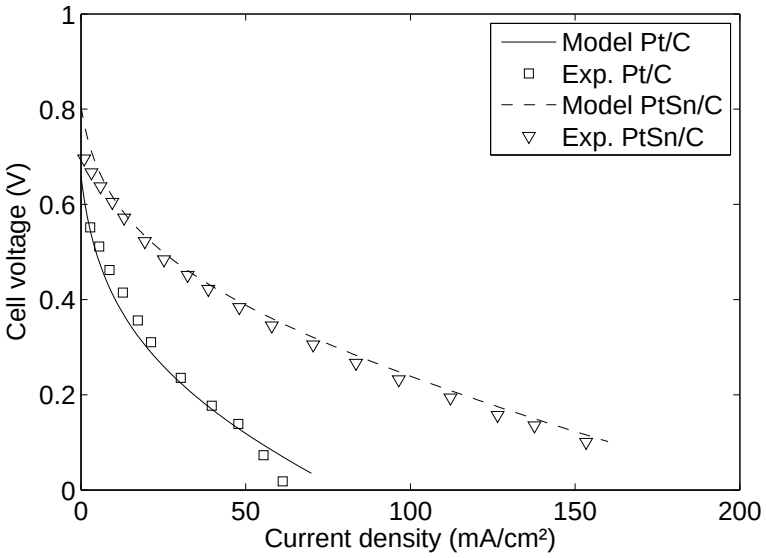

5.4 Temperature influence

The increase in temperature favors the chemical activity of the fuel and increases the conductivity of the membrane to H^+ by improving the performance of the fuel cells. The chemical activity is lower under low temperatures (273 K). High temperatures favor the process, but can reduce the life of the cells and their accessories. In this way, each type of fuel cell is designed to operate within a temperature range, so as not to compromise its energy production capacity and its useful life. PEM fuel cells typically operate between 333 K and 373 K.

The hypotheses used in the simulations were:

- Catalyst of PtRu/C at the anode and Pt/C at the cathode [7];
- Flow rate of 1 ml min^{-1} at the anode [6];
- Flow rate of 120 ml min^{-1} at the cathode [6];
- Initial pressure of 1 bar at the anode and 2 bar at the cathode [40];
- Temperatures of 333 K and 348 K;
- Initial concentration of ethanol of 1 M;
- Final time of $\tau = 30$ min [37];
- Membrane Nafion 115 [7];
- Diffusion layer porosity of $\varepsilon_d = 0.65$ [9].

Considering the PtRu/C catalyst, a study of the cell voltage was performed for two operating temperatures. Two initial temperature values were considered: 333 K and 348 K. The numerical results presented in Fig. 7 were compared with the experimental data of Andreadis and Tsiakaras (2006). The results obtained in Fig. 7 show that the fuel cell exhibits better performance at higher operating temperatures and the higher the current density, the greater the overpotential losses. There is good agreement between the experimental values and the numerical results obtained. The relative error of the model relative to the experimental data for the temperature of 333 K is 9.12% and for 348 K is 5.00%.

6 Conclusions

A numerical model for the analysis of PEM fuel cells fed by biomass derived from biomass was developed. The model considered the flow, the concentration variation of the main chemical species involved in the electro-oxidation reactions at the anode and in the electro-reduction reactions at the

Figure 7. Comparison of voltage and cell power density at two different temperatures using the PtRu/C catalyst and ethanol concentration of 1-M.

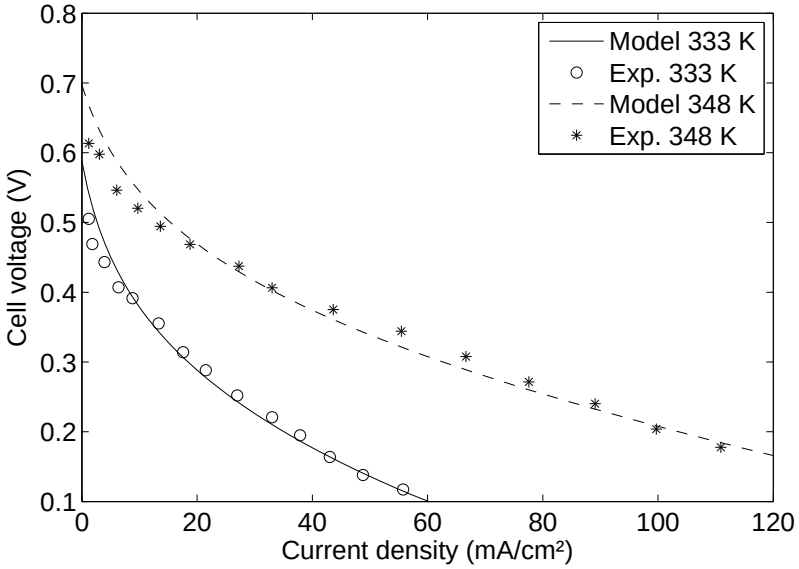

cathode, the ethanol passage through the membrane, and the main overpotential losses at the anode and at the cathode. In addition, the model is considered transient.

The flow is modeled on the Navier-Stokes equations, considering in the source term the porosity of the membrane in the diffusion and catalyst layers of the cell. The equations of chemical species consider in the source term the fuel consumption and the generation of products in the catalyst layer, according to the current density applied.

The models that calculate the overpotential losses use the parameters of velocity and concentration of the species in the catalyst modeled by the partial differential equations.

For the numerical simulation, the finite element method was used for discretization of partial differential equations in space and the Crank-Nicolson method for discretization in time. Both methods proved to be efficient in solving this problem.

The model proved to be efficient for different catalysts and operating temperatures, according to the presented results, which compare the simulations with experimental data. For future work, we intend to develop the computational code for 3D simulations and consider a multiphase model.

References

[1] Olsson, L., 2007. *Biofuels*. Advances in Biochemical Engineering/Biotechnology. Springer-Verlag Berlin Heidelberg.

[2] Lamy, C., Coutanceau, C., & Leger, J.-M., 2009. *The Direct Ethanol Fuel Cell: a Challenge to Convert Bioethanol Cleanly into Electric Energy*, pp. 1–46. Wiley-VCH Verlag GmbH and Co. KGaA.

[3] Zakaria, Z., Kamarudin, S., & Timmiati, S., 2016. Membranes for direct ethanol fuel cells: An overview. *Applied Energy*, vol. 163, pp. 334–342.

[4] Barbir, F., 2012. *PEM fuel cells: theory and practice*. Academic Press.

[5] Colmati, F., Antolini, E., & Gonzalez, E. R., 2006. Effect of temperature on the mechanism of ethanol oxidation on carbon supported Pt, Pt-Ru and Pt-3Sn electrocatalysts. *Journal of Power Sources*, vol. 157, n. 1, pp. 98–103.

[6] Andreadis, G., Podias, A., & Tsiakaras, P., 2008. The effect of the parasitic current on the direct ethanol PEM fuel cell operation. *Journal of Power Sources*, vol. 181, n. 2, pp. 214–227.

[7] Pramanik, H. & Basu, S., 2010. Modeling and experimental validation of overpotentials of a direct ethanol fuel cell. *Chemical Engineering and Processing: Process Intensification*, vol. 49, n. 7, pp. 635–642.

[8] Goel, J. & Basu, S., 2015. Mathematical modeling and experimental validation of direct ethanol fuel cell. *International Journal of Hydrogen Energy*, vol. 40, n. 41, pp. 14405–14415.

[9] Suresh, N. & Jayanti, S., 2011. Cross-over and performance modeling of liquid-feed polymer electrolyte membrane direct ethanol fuel cells. *International Journal of Hydrogen Energy*, vol. 36, n. 22, pp. 14648–14658.

[10] Abdullah, S., Kamarudin, S., Hasran, U., Masdar, M., & Daud, W., 2014. Modeling and simulation of a direct ethanol fuel cell: An overview. *Journal of Power Sources*, vol. 262, pp. 401 – 406.

[11] Gomes, R. & Bortoli, A. D., 2016. A three-dimensional mathematical model for the anode of a direct ethanol fuel cell. *Applied Energy*, vol. 183, pp. 1292–1301.

[12] Lamy, C., Lima, A., LeRhun, V., Delime, F., Coutanceau, C., & Léger, J.-M., 2002. Recent advances in the development of direct alcohol fuel cells (DAFC). *Journal of Power Sources*, vol. 105, n. 2, pp. 283–296.

[13] Rousseau, S., Coutanceau, C., Lamy, C., & Léger, J.-M., 2006. Direct ethanol fuel cell (DEFC): Electrical performances and reaction products distribution under operating conditions with different platinum-based anodes. *Journal of Power Sources*, vol. 158, n. 1, pp. 18 – 24.

[14] Kamarudin, M., Kamarudin, S., Masdar, M., & Daud, W., 2013. Review: Direct ethanol fuel cells. *International Journal of Hydrogen Energy*, vol. 38, n. 22, pp. 9438 – 9453.

[15] Heysiattalab, S., Shakeri, M., Safari, M., & Keikha, M., 2011. Investigation of key parameters influence on performance of direct ethanol fuel cell (DEFC). *Journal of Industrial and Engineering Chemistry*, vol. 17, n. 4, pp. 727–729.

[16] Abdullah, S., Kamarudin, S., Hasran, U., Masdar, M., & Daud, W., 2015. Development of a conceptual design model of a direct ethanol fuel cell (DEFC). *International Journal of Hydrogen Energy*, vol. 40, n. 35, pp. 11943–11948.

[17] Al-Baghdadi, M. A. S., 2005. Modelling of proton exchange membrane fuel cell performance based on semi-empirical equations. *Renewable Energy*, vol. 30, n. 10, pp. 1587 – 1599.

[18] Haynes, W. M., 2014. *CRC handbook of chemistry and physics*. CRC press.

[19] Le, A. D., Zhou, B., Shiu, H.-R., Lee, C.-I., & Chang, W.-C., 2010. Numerical simulation and experimental validation of liquid water behaviors in a proton exchange membrane fuel cell cathode with serpentine channels. *Journal of Power Sources*, vol. 195, n. 21, pp. 7302 – 7315.

[20] Souza, M. M., Gomes, R. S., & Bortoli, A. L., 2018a. A model for direct ethanol fuel cells considering variations in the concentration of the species. *International Journal of Hydrogen Energy*, vol. 43, n. 29, pp. 13475 – 13488.

[21] Liu, W. & Wang, C.-Y., 2007. Three-dimensional simulations of liquid feed direct methanol fuel cells. *Journal of The Electrochemical Society*, vol. 154, n. 3, pp. B352 – B361.

[22] Gomes, R. S., Souza, M. M., & Bortoli, A. L., 2018. Modeling and simulation of a direct ethanol fuel cell considering overpotential losses and variation of principal species concentration. *Chemical Engineering Research and Design*, vol. 136, pp. 371 – 384.

[23] Le, A. D. & Zhou, B., 2008. A general model of proton exchange membrane fuel cell. *Journal of Power Sources*, vol. 182, n. 1, pp. 197–222.

[24] Wang, Z. & Wang, C., 2003. Mathematical modeling of liquid-feed direct methanol fuel cells. *Journal of the Electrochemical Society*, vol. 150, n. 4, pp. A508–A519.

[25] Atkins, P., Jones, L., & Laverman, L., 2012. *Chemical Principles*. W. H. Freeman.

[26] Jeng, K. & Chen, C., 2002. Modeling and simulation of a direct methanol fuel cell anode. *Journal of Power Sources*, vol. 112, n. 2, pp. 367–375.

[27] Bard, A. J., Faulkner, L. R., et al., 2001. *Electrochemical Methods: Fundamentals and applications*.

[28] Yuan, X.-Z. R., Song, C., Wang, H., & Zhang, J., 2009. *Electrochemical impedance spectroscopy in PEM fuel cells: fundamentals and applications*. Springer Science & Business Media.

[29] Farhat, Z. N., 2004. Modeling of catalyst layer microstructural refinement and catalyst utilization in a PEM fuel cell. *Journal of Power Sources*, vol. 138, n. 1-2, pp. 68–78.

[30] Ge, J. & Liu, H., 2006. A three-dimensional mathematical model for liquid-fed direct methanol fuel cells. *Journal of Power Sources*, vol. 160, n. 1, pp. 413–421.

[31] Kareemulla, D. & Jayanti, S., 2009. Comprehensive one-dimensional, semi-analytical, mathematical model for liquid-feed polymer electrolyte membrane direct methanol fuel cells. *Journal of Power Sources*, vol. 188, n. 2, pp. 367–378.

[32] Cussler, E., 1997. *Diffusion:*. Cambridge Series in Chemical Engineering. Cambridge University Press.

[33] Scott, K., Argyropoulos, P., & Sundmacher, K., 1999. A model for the liquid feed direct methanol fuel cell. *Journal of Electroanalytical Chemistry*, vol. 477, n. 2, pp. 97–110.

[34] Tayal, J., Rawat, B., & Basu, S., 2012. Effect of addition of rhenium to Pt-based anode catalysts in electro-oxidation of ethanol in direct ethanol PEM fuel cell. *International Journal of Hydrogen Energy*, vol. 37, n. 5, pp. 4597 – 4605.

[35] Andreadis, G. & Tsiakaras, P., 2006. Ethanol crossover and direct ethanol PEM fuel cell performance modeling and experimental validation. *Chemical Engineering Science*, vol. 61, n. 22, pp. 7497–7508.

[36] Souza, M. D. & Bortoli, A. D., 2019. Stability and convergence of the numerical solution for the species equation of a model for PEMFCs. *Computers & Mathematics with Applications*, vol. 77, n. 4, pp. 1197 – 1215.

[37] Park, Y.-C., Kim, D.-H., Lim, S., Kim, S.-K., Peck, D.-H., & Jung, D.-H., 2012. Design of a MEA with multi-layer electrodes for high concentration methanol DMFCs. *International Journal of Hydrogen Energy*, vol. 37, n. 5, pp. 4717 – 4727.

[38] Goel, J. & Basu, S., 2014. Effect of support materials on the performance of direct ethanol fuel cell anode catalyst. *International Journal of Hydrogen Energy*, vol. 39, n. 28, pp. 15956 – 15966.

[39] Antolini, E., 2007. Catalysts for direct ethanol fuel cells. *Journal of Power Sources*, vol. 170, n. 1, pp. 1–12.

[40] Song, S., Zhou, W., Tian, J., Cai, R., Sun, G., Xin, Q., Kontou, S., & Tsiakaras, P., 2005. Ethanol crossover phenomena and its influence on the performance of DEFC. *Journal of Power Sources*, vol. 145, n. 2, pp. 266 – 271.